Electronic Supplementary Material (ESI) for Analytical Methods.

SUPPLEMENTARY INFORMATION

Trace gas and dynamic process monitoring by Raman spectroscopy in metal-coated hollow glass fibres

Timothy M. James *[a], Simone Rupp [a] and Helmut H. Telle [b]

[a] *Institute for Technical Physics (ITEP), Tritium Laboratory Karlsruhe (TLK), Karlsruhe Institute of Technology (KIT), P.O. Box 3640, 76021 Karlsruhe, Germany. E-mail: Timothy.James@kit.edu.*

[b] *Instituto Pluridisciplinar, Universidad Complutense de Madrid, Paseo Juan XXIII-1, 28040 Madrid, Spain.*

CONTENT

S1. Fluorescence background and its minimisation

To minimise the fluorescence background the sources of the fluorescence need to be considered carefully, and measures be taken to eliminate the causes as much as possible. Considerations need to be given (i) to the optics in the laser beam path; (ii) to their material of manufacture and their thickness; (iii) to the interaction of laser light with the glass capillary; and (iv) to the coupling of laser light into the capillary core. Here we provide some additional information beyond that included in the main manuscript, specifically addressing results from our systematic studies.

S1.1 Optical components in the laser beam path

In backward Raman setups, as implemented for our capillary configuration, the optical components exposed to laser radiation are the dichroic beam splitter to separate laser from Raman radiation, focussing and collection lenses, and the Raman cell window(s).

For the results described below the dichroic mirror was always in place. However, we are currently exploring a number of alternatives which will allow one to overcome the associated florescence problem, at least in part.

In the early stages of our capillary Raman implementation a joint laser focussing / Raman light collection lens was used, in the form of an achromatic lens with suitable anti-reflection coating. It was thought at the time that it was important that the light striking the dichroic mirror should be as close as possible collimated, i.e. well within the angular specification tolerance recommended for best performance of this component. However, this single-lens configuration on the one hand limited the setup flexibility, and on the other hand introduced a substantial amount of fluorescence. The latter can be traced to the non-optimal material of achromatic doublets, normally made from two different materials with compensating refractive index, namely F2-flint and BK7 glasses (for material issues see Section S1.2 further below).

Fluorescence reduction has been achieved by moving the collection lens behind the beam splitter and using a second lens, with a longer focal length, to focus the laser light into the capillary. Backward Raman spectra of air were taken with the two collection-lens configurations (in front of and behind the beam splitter) with the collection system comprising the PI Acton *SP500i* spectrometer and the Horiba *Synapse* CCD detector.

Spectra recorded with either of the two lens configurations are shown in Figure S1. The data clearly show that the

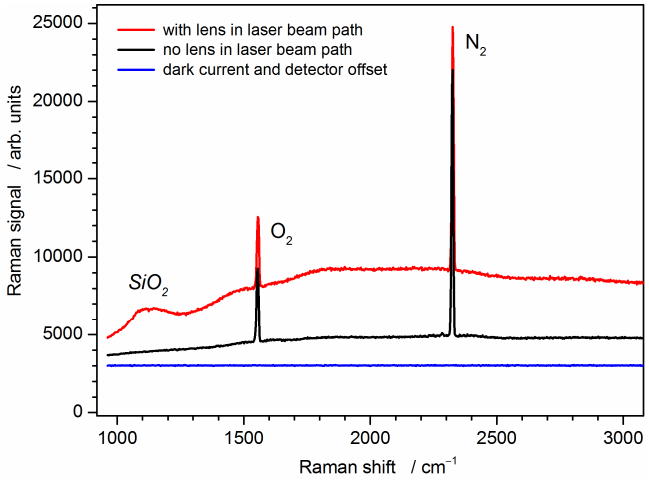

Figure S1: Backward 180° Raman spectra of air, with the focussing lens in front of and behind the dichroic beam splitter. In both setups the focal length of the light collection lens is f = 150 mm. The spectrum acquisition time was 10× 1 s. Note that the fluorescence background has not been removed; the blue line corresponds to the zero-signal dark current and the detector offset.

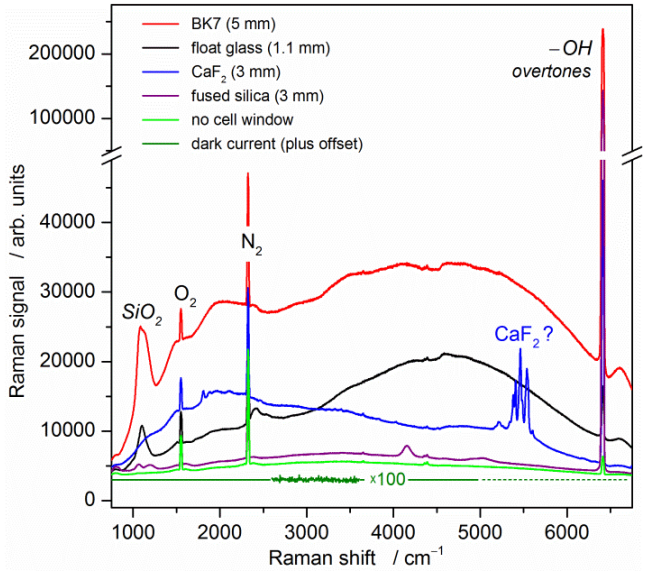

Figure S2: Backward Raman spectra of air, with windows of different optical materials placed in the laser excitation / Raman light collection beam paths. The setup was the same as for the measurements discussed in Section S1.1, but the spectrum acquisition time was only 5 s. Note the fluorescence background has not been removed; the flat trace corresponds to the zero-signal dark current and the detector offset.

magnitude of the fluorescence background reduces drastically by moving the f = 150 mm achromatic collection lens (which also served as the focussing lens for the laser) behind the beam splitter, i.e. out of the laser beam path. Of course, this means that a second lens is required for focussing of the laser light. At the same time this provides the freedom to independently adjust the focal length (in the case shown to f_L = 400 mm) for optimum coupling to the Raman medium, whilst enabling the solid angle for light collection to be maximised using a different (shorter) focal length lens. Note that this becomes more important in capillary-type measurements, where a narrow solid angle for the laser light is required to maximise the coupling of the laser beam to the hollow glass fibre and minimise its interaction with the capillary glass body. Note that the flat baseline (no fluorescence) constitutes the dark current signal, with the laser off, plus the detector offset voltage.

To quantify the gain in the signal-to-noise ratio (SNR) by moving the collection lens behind the beam splitter, the fluorescence background has been removed, and the SNR related to the two configurations has been extracted from the respective spectra. For simplicity, the Raman signal is taken as the height of the Q_1-branch of nitrogen above the background, and the noise as the standard deviation of a flat region of the background-subtracted spectra. The resultant SNRs of the two setups are 328 and 700, respectively. This shows that by moving the lens behind the beam splitter the fluorescence contribution (to the noise) from the optics in the beam path has been reduced by approximately a factor of 2.

As a consequence of these measurements, from here onward the light pass between the dichroic beam splitter and the cell / capillary window was kept free of the laser focussing and Raman light collection lenses, as well as any other optical component. Note however that the fluorescence contribution from the beam splitter always persists.

S1.2 Optical materials and their thickness

In order to determine whether further reductions in fluorescence are feasible, it is important to pin-point its origins, and how component properties relate to its magnitude. The two main variables, related to photon – matter interaction, of any optical element are the material and the thickness of the component. The common optical materials used in visible Raman spectroscopy are borosilicate glass, BK7; fused silica; and calcium fluoride, CaF_2. In addition, we also tested float glass, which is occasionally found in low-cost fluorescence cells.

To trace the influence of each optical material, measurements have been performed in which windows made from these three materials have been placed in the beam path between the Raman scattering region and the collection optics, and were exposed to laser radiation, ensuring the window was installed in the same location for each measurement. Raman spectra of air were recorded, for the range up to about 7000 cm^{-1}, to reveal the materials' influence on the observed spectrum background (see Figure S2). All tests were performed under the same laser excitation and Raman light detection conditions.

Measurements were performed without any window; a 1.1 mm thick float glass window (*Knight Optical* WGW2522-AV2); a 5mm thick BK7 window (*ThorLabs* WG11050-A); a 3mm thick calcium fluoride window (*INGCRYS*, custom made); and a 3mm thick fused silica window (*Knight Optical* WHQ2500). The spectra in Figure S2 show that all optical components introduce a fluorescence background to the (backward) Raman spectrum. On the arbitrary - but normalised - scale, the observed fluorescence of the fused silica window was the smallest. For example, at 3500 cm^{-1} in the

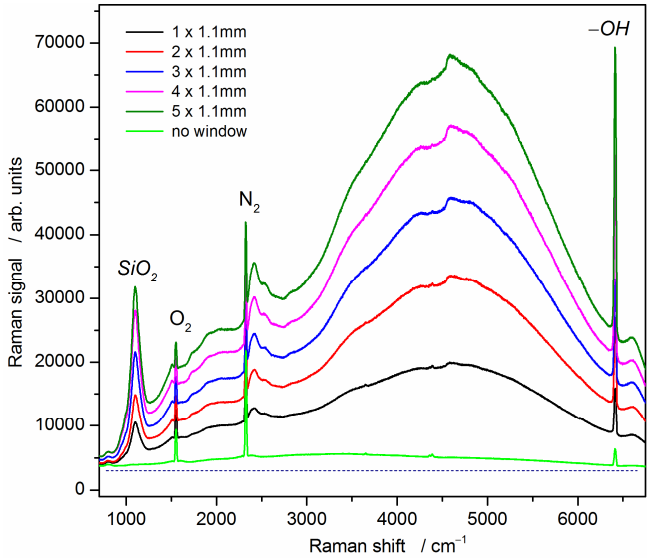

Figure S3: Backward Raman spectra of air with different numbers of float glass windows placed in the beam path. The acquisition time was 10× 5 s; in the setup the focal length of the Raman collection lens was f = 150 mm. Note that the fluorescence background has not been removed; the dotted (grey) line indicated the dark current background and detector offset.

spectrum, it lies only marginally above the dark current / detector offset baseline. It is followed (at the same spectral position) by the calcium fluoride window; then the float glass window; and finally the BK7 window. All materials exhibit substantially larger fluorescence than fused silica.

On first sight, the observed order was slightly counter-intuitive to statements on optical materials, as normally found in the Raman literature. However, the fluorescence contribution scales about linearly with optical thickness (as is shown further below). Thus, one may normalise the fluorescence increase to that of a window with thickness 1 mm. This would change the order of fluorescence contribution to the expected one (lowest to highest): fused silica; calcium fluoride; BK7; and float glass. Note that the fluorescence maximum for each optical material is not at the same spectral location.

In addition, the optical components introduce additional spectral features, not only related to fluorescence but also to material-related Raman features. The most obvious of these features is the large, common peak at around 6400 cm^{-1}. Note that this is also present for spectra recorded with no window in the beam path, but its intensity is enhanced by the addition of the windows. This peak can be associated with symmetric / asymmetric stretch combination bands of –OH in host matrices. [1] While this feature is outside the standard range used in fundamental-vibration Raman spectroscopy, it provides a clear link to the water content in each optical material – normally indicative of the manufacturing process.

At the other end of the displayed spectral range one encounters a broad feature at around 1100 cm^{-1}; this is normally attributed to the Si–O–Si stretch vibrations in polymerised bulk-SiO_2. [2,3]

As expected, the SiO_2 bands are not observed in calcium fluoride, but besides its strong, broad fluorescence it features quite a few Raman peaks in the spectral range 1500-3500 cm^{-1} (associated with CaF_2 overtone vibrations), which – although small – are nevertheless detrimental when exacting quantitative trace gas analysis. In addition, one observes a series of distinctive peaks in the range 5400-5600 cm^{-1}; these can most likely be attributed to impurities in the bulk material (rare earth and F_2-centre transitions). [4]

As stated above, the thickness of the optic also influences the actual fluorescence amplitude. In order to systematically check this effect, which should be roughly linear for not-too-thick samples, measurements were carried out using a stack of 1.1 mm float glass windows (*Knight Optical* WGW2522-AV2, AR-coated 450-900 nm) in the beam path. These windows were added one by one to systematically determine the increase in the fluorescence (and the system noise) with respect to the thickness of the material. The related spectra are shown in Figure S3. The fluorescence level clearly increases as the material thickness goes up, as do the SiO_2 feature at 1100 cm^{-1} and the –OH overtone peak at 6400 cm^{-1}; all these are related to the window material properties. The Raman peak of the molecular components in air, O_2 and N_2, are not affected.

To determine the relationship between optical component thickness and fluorescence level (Y), the noise (N_Y) introduced by the increase in fluorescence background was extracted from the spectra. For this, the background was removed and the standard deviation of a then flat region between peaks was calculated at different Raman shift locations. The noise introduced by an increasing background height is caused by shot noise ($\sqrt{Y}$); therefore, if the fluorescence height increases linearly with respect to optical component thickness, one would expect the gain in noise to be equal to the square root of the thickness. While the noise fluctuations are not visible on the scale of Figure S3, the data yielded the expected relation. For the stepwise increase in the thickness of the window stack one expects the relation

$$(\text{Noise } s\times 1.1\text{mm} \,/\, \text{Noise } 1\times 1.1\text{mm}) \approx \sqrt{n} \quad .$$

For example, for a stack of five windows (s = 5) we calculated from the experimental data a noise increase of 2.37 ± 0.28; this is in line with the expected value of $\sqrt{5} = 2.23$,

As a consequence of these material and thickness measurements, for lowest fluorescence background one should (i) chose fused silica windows / optics; (ii) select their thickness as thin as is practically possible; and (iii) reduce the number of components to a minimum, whose fluorescence would be captured by the Raman light collection.

S1.3 Caps to protect the capillary walls from direct exposure to laser light

To minimise the fluorescence contribution from light leakage into the glass walls of the capillary, a "cap" design was implemented in this work. The capillary with an outer diameter of 1.6 mm was inserted into this cap to position it laterally, with a precision of about ±0.05 mm. To be effective, the centre aperture of the cap needed to be matched to the capillary's inner diameter of 1.0 mm, i.e. it had to be marginally smaller. Dictated by the manufacturing precision the cap's aperture lateral offset tolerance was nominally 0.1 mm. This meant that in unfavourable cases the aperture might be

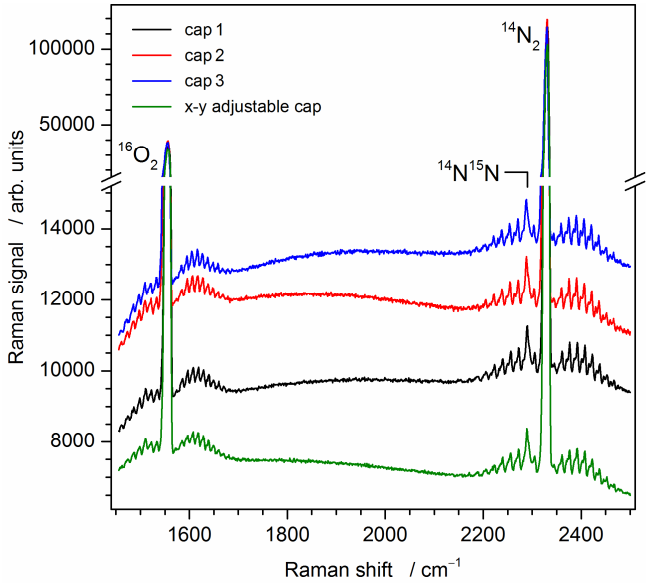

Figure S4: Capillary Raman spectra of air at atmospheric pressure, recorded for three different caps with 0.8 mm aperture. A measurement using a x-y-adjustable cap with a 0.8 mm pin-hole is shown for comparison. All spectra are averages of 10 back-to-back recordings with 2 s acquisition time.

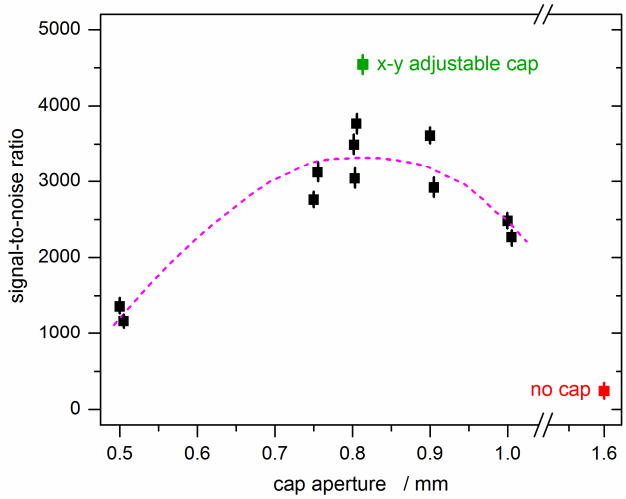

Figure S5: Signal-to-noise ratio for the N_2 Q_1-branch peak, recorded at atmospheric pressure, for different cap aperture diameters. Additional data for no cap and an x-y adjustable cap of 0.8 mm aperture are included for comparison. Note that data points for repeat measurements are displaced sideways for clarity; the dashed line is for guidance only.

off-centre, and thus the cap would not completely shield the glass body from exposure to laser radiation.

Caps with different aperture diameter were made, with full 1.0 mm and reduced apertures down to 0.5 mm, to determine the optimum value at which the fluorescence contribution from the capillary would be minimal without restricting the collection of Raman light. Note that for each aperture diameter more than one cap was manufactured and tested, in order to ascertain tolerances in aperture precision and capillary positioning during insertion.

The process of minimising the fluorescence and at the same time trying to not significantly affect the Raman signal should be mirrored in the SNR, and thus the achievable limit of detection. In Figure S4 spectra for three caps with the same aperture diameter of 0.8 mm are shown. These clearly demonstrate the effect of manufacturing and capillary-insertion tolerances; normally, the cap with the best fluorescence suppression was selected for further measurements.

For each cap aperture the SNRs of the measurement tests were calculated from spectra similar to those shown in Figure S4. These spectra were processed for cosmic ray removal and fluorescence background subtraction (as described in the main manuscript text). The maximum amplitude of the N_2 Q_1-branch was then taken as the signal (for simplicity), and the noise was calculated as the standard deviation of a flat region in the spectrum. At least two caps were manufactured and tested for each aperture diameter; results from this measurement series are shown in Figure S5. The tolerance of caps with the same aperture diameter is reflected in the scatter of the related SNRs, but a clear trend is evident from the data, namely that for the largest and smallest apertures the SNR is reduced. In the former case the fluorescence is not optimally suppressed, while in the latter case the collection of Raman light is restricted.

In addition to the spatially fixed caps an x-y adjustable cap design was considered, which would allow one to compensate for the lateral tolerances associated with the manufacture of the caps. The concept principle was tested using an "open-capillary" (no cell) setup, in which the cap was replaced by a 0.8 mm precision pinhole, installed into an x-y adjustable mount at the location of the ordinary cap assembly, as shown in Figure S6.

First, the laser beam was aligned to optimally enter the capillary by monitoring the shape of the transmitted laser beam profile. Then the pinhole position was adjusted so that the laser beam profile was not adversely affected and that the observed fluorescence amplitude in the (real-time) Raman spectrum from the capillary became minimised. Thus, the SNR reaches its maximum. The improvement of using an adjustable cap is evident when comparing the

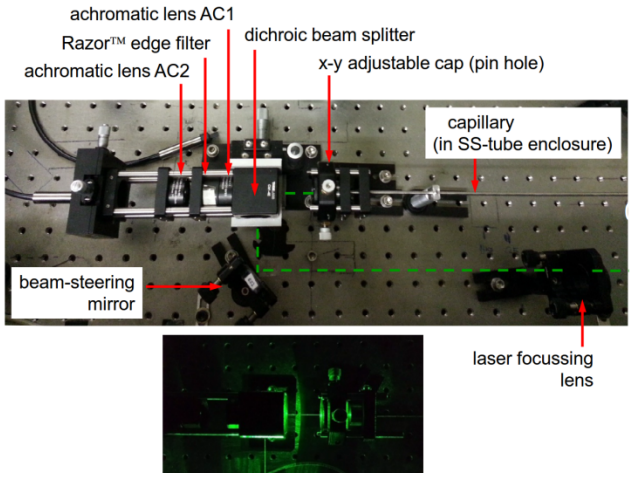

Figure S6: Setup for testing the adjustable-cap capillary Raman configuration.

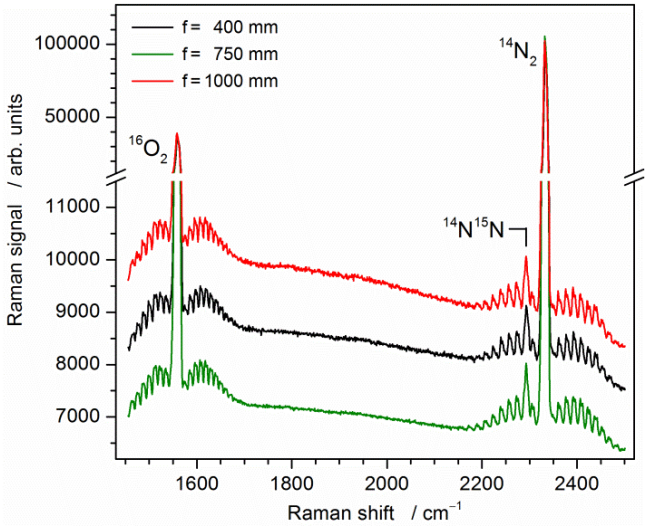

Figure S7: Capillary Raman spectrum of air at atmospheric pressure, for laser coupling lenses with different focal length. The spectra are averages of 10 back-to-back acquisitions, with an acquisition time of 2.5 s.

Raman spectra and SNR with the data from the different fixed caps (recorded under the same measurement conditions). The resulting, improved spectral and SNR data are included in Figures S4 and S5 for comparison.

Finally, we would like to note that introducing a cap, or other means – like our pinhole approach or the coating of the capillary end faces with a silver metal layer,[5] is essential to protect the glass capillary body from exposure to laser radiation, and thus the generation of strong fluorescence. The fluorescence background without protection can become even larger than the Raman signal itself, and the SNR is severely lowered. This adverse case is quite evident from the related (red) data point included in Figure S5.

S1.4 Coupling of laser light into the hollow fibre core

As discussed by various authors, mode and beam waist matching of the laser beam to the capillary is essential (see e.g. Mullen *et al* [5]) to optimise the coupling of the laser light into the capillary. Hand in hand with this optimal coupling goes a reduction of light leaking into the glass of the capillary, which as a consequence increases the fluorescence background. In the simplest case, near-optimal coupling can be achieved by appropriately selecting the focal length and position of the lens used to focus the laser radiation into the capillary.

Test measurements have been performed with capillaries of different length (200 mm and 650 mm, respectively) to try and select the focal length of the lens to optimise the Raman detection limit, i.e. to maximise the SNR. Besides the initial short-focus lenses, which proved to be rather inefficient, we used laser focussing lenses with f = 400 mm, 750 mm and 1000 mm; their position relative to the capillary was adjusted so that the minimal beam waist at the focus point coincided roughly with the half-length of the capillary. For each lens 10 back-to-back Raman spectra of air were measured. As is the case in all other fluorescence suppression measures discussed above, the increase in SNR is linked to the suppression in the fluorescence background (see the example spectra in Figure S7).

The figure shows that the highest SNR is achieved when using the f = 750 mm lens; for both the shorter and longer focal lengths the SNR is less. Note that this focal length should not be seen as a "universal" value but only applies to the lasers utilised by our group, as the focussing angle from a lens is also dependent on beam size and beam divergence of the light incident onto the lens. This test would need to be repeated in the case that the laser was changed, to verify whether the same focal length would maintain the optimal coupling.

Finally, we also checked the dependence of the SNR on the acquisition time. While the amplitude of both the Raman and fluorescence signals should increase proportionally with acquisition time, as long as the detector does not saturate, the shot noise changes as the square root of the signal. Therefore, the SNR should reflect this behaviour.

Spectra of air at atmospheric pressure were recorded for a range of acquisition times, using the three focal length lenses mentioned above. As outlined in the main text, the *LARAsoft* package [6] was used to process the spectra and then calculate the signal and noise of the Q_1-branch of N_2. The calculated SNRs are shown in Figure S8, as a function of acquisition time. Clearly, the plotted data follow the expected trend (the SNR should rise proportional with the square-root of acquisition time), and confirm that the SNR is largest for the lens with f = 750 mm.

S1.5 Summary effect of all improvement measures

When all measures described in sections S1.1 to S1.4 were implemented the SNR of our capillary Raman system increased at least threefold in comparison to setup configurations without them. Notably (i) we reduced the optical elements exposed to the laser excitation beam to two, i.e. the dichroic beam splitter (*Semrock* Di02-R532-25x36, substrate

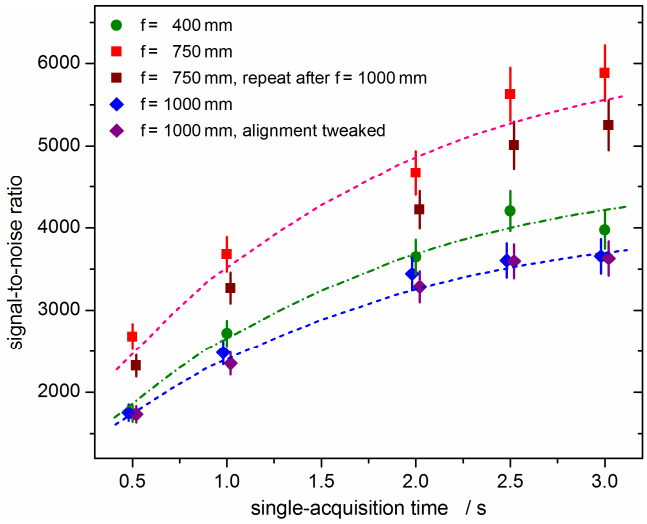

Figure S8: Signal-to-noise ratio (SNR), as a function of acquisition time, for laser lenses with different focal length. The dashed lines are fits to a function $f(t) \propto \sqrt{t}$..

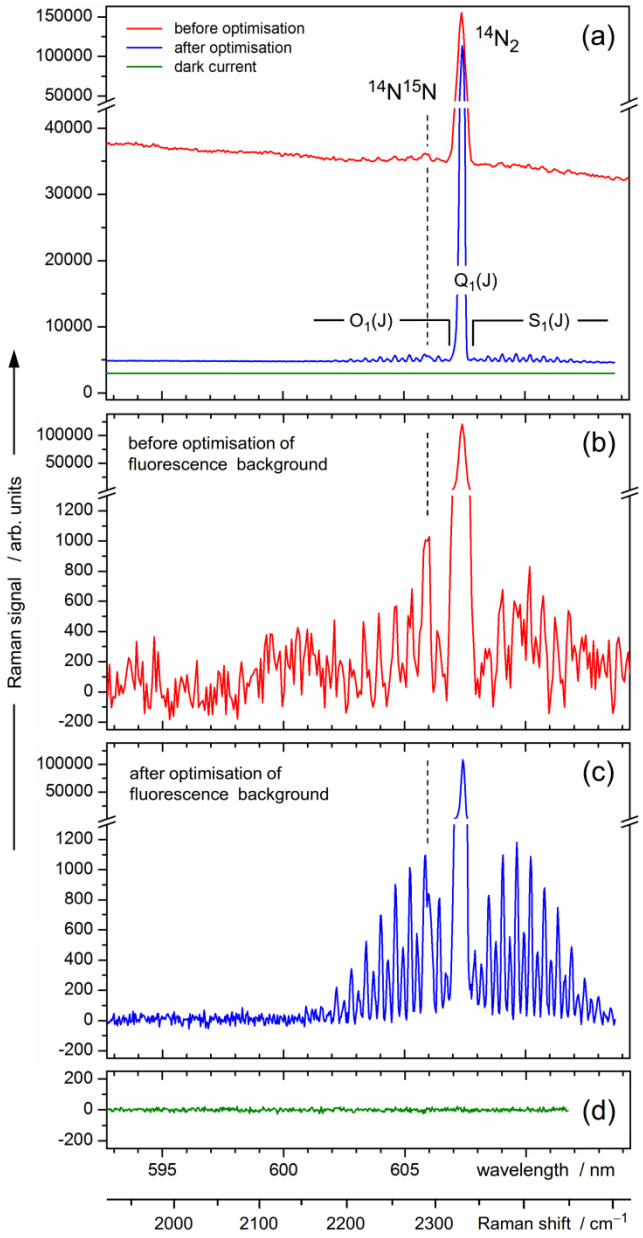

Figure S9: Full comparison before / after fluorescence optimisation, exemplified for the Raman spectrum of air at atmospheric pressure. Panel (a) – spectral traces including the fluorescence background; panels (b) and (c) – fluorescence background removed, using *LARAsoft;* panel (d) – detector dark current.

thickness 1 mm) and the capillary cell window (BBAR-coated fused silica substrate with 2 mm thickness); (ii) a protective cap with 0.8 mm aperture was used as standard, shielding the glass capillary face from direct exposure to laser radiation; and (iii) the laser focussing lens was selected to optimally couple the radiation into the capillary, so that interaction with the capillary walls was minimised.

In Figure S9 the overall effect of the fluorescence reduction measures is demonstrated for a typical prior / post optimisation measurements. The prior-optimisation setup utilised an achromatic lens with f = 150 mm for laser focussing and Raman light collection; a cell window of thickness 3 mm; and a capillary cap with 1 mm aperture. In the post-optimisation configuration the laser focussing and Raman light collection lenses were separate and removed from direct exposure or line-of-sight, with f_{laser} = 750 mm and f_{Raman} = 75 mm; the thickness of the cell window was reduced to 2 mm; and the cap aperture was 0.8 mm. All other experimental instruments and parameters were the same (laser power, spectrometer, detector, acquisition time), except for a slightly different slit width of the spectrometer.

Table S1: Relevant parameters of the spectrometer and detector instrumentation used in this study.

Spectrometer	**PI Acton *SP500***	**PI Acton *SP2150***
Focal length	500 mm	150 mm
Aperture ratio	f/6.5	f/4
Grating size	68×68 nm	32×32 nm
Efficiency at 620nm:		
600 gr/mm blaze 300 nm	~30 %	~30 %
600 gr/mm blaze 500 nm	~62 %	~62 %
1200 gr/mm blaze 750 nm	~80 %	~80 %
2400 gr/mm blaze 300 nm	~35%	~35%

Detector	**Horiba *Synapse***	**Princeton *Pixis 400B***
Type	FIOP	back-illuminated
Pixel number	1024×256	1340×400
Pixel size	26×26 μm	20×20 μm
Cooling temperature	-70 °C	-73 °C
Dark current	0.002 e/pixel/s	0.001 e/pixel/s
QE at 620 nm	~43 %	~96 %

It should be noted that the suppression of fluorescence background is incomplete since the capillary cell window is always present for closed volume configurations. Equally, the dichroic mirror was always in place although we are currently testing promising alternatives which would allow nearly full removal of its contribution to the fluorescence background.

Finally, the improvement in SNR and thus detection limits can be influenced by the choice of spectrometers and/or detectors. While it may not be possible to change equipment at will, but the choice may be dictated by available instruments or budget constraints, it is nevertheless often possible to configure a system in such a way that the accumulated signal exhibits the best possible magnitude. In Table S1 the vital parameters of the spectrometer and detector systems available in this study are collated. Those data suggest a difference in light collection of about 16, between the "worst" and "best" combination of components; thus a fourfold increase in SNR might be achievable.

S2. Detection limits for molecular species

As stated in the main text, a direct comparison between capillary Raman, standard 90° (sideways) and 180° (backward) implementations - the latter two without any cell - was

Table S2: Measured Raman signal, noise and SNR of the N_2 Q_1-branch obtained using capillary, 180° and 90° Raman configurations. The uncertainties in the last digit are given in brackets.

Time /s	Signal	Noise	SNR	SNR gain vs 90° config
	90°			
0.1	32 (3)	2.2 (2)	15 (2)	
0.2	64 (4)	2.8 (4)	23 (4)	
0.5	156 (6)	2.6 (2)	61 (5)	
1	324 (9)	2.5 (2)	128 (11)	
2	616 (12)	2.7 (3)	225 (25)	
	180°			
0.1	497 (11)	3.4 (4)	146 (18)	9.7 (18)
0.2	994 (15)	3.8 (6)	264 (42)	11.5 (27)
0.5	2497 (25)	6.8 (7)	365 (37)	6.0 (8)
1	4863 (35)	10.8 (11)	450 (46)	3.5 (5)
2	9757 (49)	12.0 (13)	810 (87)	3.6 (6)
	capillary			
0.1	5507 (37)	17.6 (25)	314 (45)	20.9 (41)
0.2	10918 (52)	19.8 (37)	550 (103)	23.9 (61)
0.5	26550 (82)	30.5 (46)	872 (132)	14.3 (26)
1	53397 (116)	39.0 (83)	1371 (292)	10.7 (25)
2	106607 (163)	54.0 (96)	1973 (351)	8.8 (18)

made. The same laser and spectrometer / detector settings were applied, and data were recorded for acquisition times between 0.1 and 2 s for all three setup implementations, averaging five consecutive measurements for each case (a comparison spectrum for the 2 s acquisition time was shown as Figure 4 in the main text). The Raman signal amplitude was extracted from the height of the Q_1-branch of nitrogen, and the noise as its standard deviation from a flat region of the background. The detection limit improvement was determined by calculating the SNR for each experimental setting. The results from all data sets are collated in Table S2.

The table shows that Raman signal gains of ~170 and ~10 were obtained for all acquisition times, when using the capillary implementation instead of the standard 90° and 180° implementations, respectively. However, both backward collection configurations exhibited substantially increased noise, due to the fluorescence generated in the optical components in the laser beam path and/or the capillary. Thus, when taking the shot noise level into account, one finds that the achieved detection limit improvement is far less than the signal amplitude gain implies. The related improvements in SNR for the two backward implementations over the 90° configuration are collated in the final column of Table S2. These results clearly emphasise the need to understand and minimise fluorescence background contributions in all backward collection configurations.

Note that the data collated in Table S2 was taken before the fluorescence background reduction techniques, discussed in Section S1 of this supplement, were implemented. This means that the achievable detection limit improvement in our final system implementation should be substantially

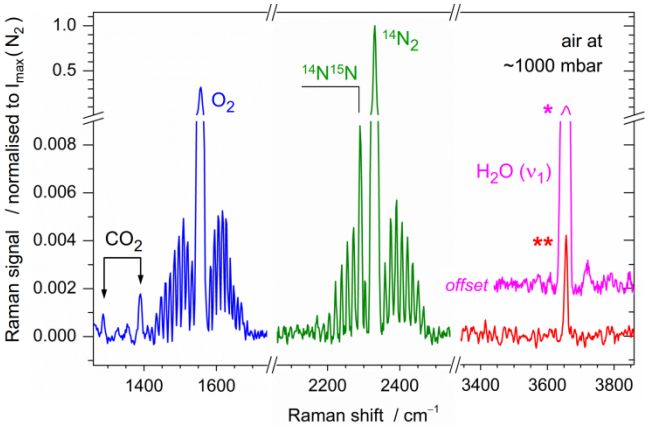

Figure S10: Capillary Raman spectrum of air at atmospheric pressure, for an acquisition time of 100x 2 s (background subtracted). The Q_1-branches of all relevant major and minor molecular components are annotated. * = data from dry (dehumidified) KIT laboratory; ** = data from Swansea laboratory.

higher, albeit still lower than the signal amplitude enhancement would suggest. Note also that different spectrometer / detector combinations would influence the actual signal strength only.

S2.1 Atmospheric gases

A capillary Raman spectrum of ambient air was recorded to verify the sensitivity of the system as explained in the main manuscript. For clarity, the capillary Raman spectrum of air from the main text (Figure 3) is repeated here as Figure S10.

The magnitude of the observed Raman signal of nitrogen (N_2), oxygen (O_2), carbon dioxide (CO_2), water (H_2O) and the minor isotopologue $^{14}N^{15}N$ can be extracted as the height of the Q_1-branch peaks above the noise level; these values are collated in Table S3. The ratio of these branches with respect to the Q_1-branch of nitrogen was calculated. However, in order to compare the obtained values with those in the literature the Raman cross section and spectral response need to be taken into account for each constituent. The relevant cross sections, σ_i, with respect to the cross section of nitrogen are included in the table (these values are obtained from Danichkin *et al* [7] and Penney *et al* [8]).

The Raman intensity can be expressed in terms of the spectral response as

$$I = \sigma n V D$$

where σ is the Raman scattering cross section; n is the number of interacting molecules; V is the scattering volume; and D includes a set of constants that are independent of the scattering substance. If two gases are present in the same Raman measurement V and D are the same. Thus, the ratio of said two Raman intensities leads to

$$\frac{I_1}{I_2} = \frac{\sigma_1 n_1}{\sigma_2 n_2} \quad .$$

This equation can be used to obtain the required composition ratio (n_1/n_2) and these values are tabulated in the last column

Table S3: Measured signal and composition (relative to the N_2 Q_1-branch) of the observed Raman Q_1-branches; the data are based on an averaged capillary Raman spectrum of air (100x 2 s). σ_i = Raman scattering cross section; n_i = number of interacting molecules.

Q_1-Peak	Signal	Ratio to $^{14}N_2$	σ_i/σ_{N2}	n_i/n_{N2}
$^{14}N_2$	122322 (350)	1.00000 (286)	1.00 (0)	1.00000 (286)
$^{14}N^{15}N$ [(a)]	905 (67)	0.00740 (55)	1.00 (0)	0.00740 (55)
O_2	39034 (198)	0.31910 (168)	1.23 (6)	0.2594 (155)
CO_2 (ν_1)	217 (23)	0.00178 (19)	1.51 (9)	0.00118 (15)
CO_2 (ν_2)	115 (23)	0.00094 (19)	1.00 (10)	0.00094 (21)
H_2O [(b)]	540 (36)	0.00441 (29)	2.50 (25)	0.00176 (21)
H_2O [(c)]	6165 (81)	0.05037 (72)		0.02015 (203)
noise	23 (5)	0.00019 (4)	– NA –	– NA –

[(a)] The $^{14}N^{15}N$ data are deconvoluted from the $O_1(J)$ branch of $^{14}N_2$.
[(b)] Data recorded in air-conditioned (dehumidified) lab
[(c)] Data recorded in humid lab (at Swansea)

of Table S3, with n_2 associated with the reference molecule nitrogen.

The generally accepted values for the composition of dry air are 0.78082(12) for nitrogen, 0.20945(12) for oxygen and 0.00039(1) for carbon dioxide.[9] These values can be converted to relative compositions, with reference to nitrogen, yielding 1.00000 (22), 0.26824 (16) and 0.00050 (1), respectively, which can be compared to the experimental data in the last column of Table S3.

Inspecting the results collated in Table S3 the following observations can be made.

Firstly, the derived abundance of $^{14}N^{15}N$ in air is in reasonable agreement with the published reference value 0.00728 (30).[10] Note here that its Q_1-branch overlaps with some of the $O_1(J)$ lines of $^{14}N_2$; and deconvolution was required, for example following the procedure described in James *et al* [11]: (i) fit the free-standing $O_1(J)$ lines of $^{14}N_2$; (ii) generate a synthetic $O_1(J)$-branch from the fit; (iii) subtract this from the experimental spectrum, the remainder being the Q_1-branch of $^{14}N^{15}N$.

Secondly, the relative composition of oxygen, extracted from the measured Raman spectra, agrees with the expected value within its experimental uncertainty.

Thirdly, the measured value for carbon dioxide is out by approximately a factor of about two - both when derived from the ν_1- or ν_2-bands. This can be linked to the fact that the wavelength dependent spectral response of the light collection and detection systems were not taken into account. To correct for this discrepancy the system response function would have to be calibrated. This has already been achieved for our standard 90° detection systems at TLK, based on a procedure described in Schlösser *et al*. [12] A similar approach suitable for capillary-type systems is under investigation. In addition, the carbon dioxide concentration may differ slightly from the average global concentration over a period of a day depending on the lab location and the number of people working in the laboratory as discussed in the main manuscript. However, the measured increase is much smaller than the discrepancy measured here, which further indicates that the system spectral response function will need to be determined to accurately calibrate the system.

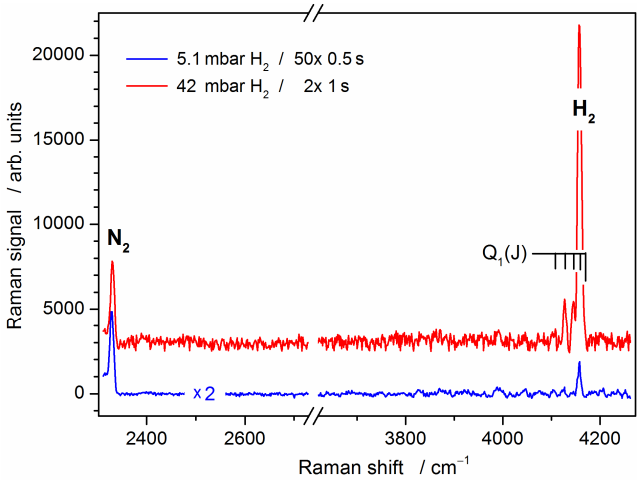

Figure S11: Example capillary Raman spectra of low-pressure H_2 fillings (background subtracted; offset for clarity), also demonstrating the effects of signal acquisition time and averaging. Note that the nitrogen signal stems from atmospheric air outside the capillary cell.

Finally, the measured concentration of water vapour is well within the range normally encountered in ordinary laboratory conditions, with and without dehumidification. For example, applying standard conversion procedures based on molecular weights, one derives from the data shown in Figure S10 and Table S2 that the water vapour content in the air of our Swansea lab was about 11.7 ± 1.5 g·m^{-3}. Using relative humidity tables [13] this converts into a value of about 65 %, at a lab temperature of ~20 °C. This is within the range 60-80 % tabulated in the associated daily weather record.

S2.2 Hydrogen isotopologues

In addition to the atmospheric gases, capillary Raman spectra of different, well controlled mixtures of hydrogen isotopologues were recorded. The measurements were performed for a range of filling pressures, ranging from isotopologue mixtures of up to 1000 mbar down to low-pressure fillings of just about 5 mbar of pure hydrogen.

Examples for some low partial-pressure hydrogen spectra are shown in Figure S11; these examples also demonstrate the effects of different acquisition times and spectral averaging. For simplification, the total H_2 signal was approximated by using the strongest $Q_1(J=1)$ line amplitude only. Based on this approximation one finds for the 5 mbar case a limit of detection (LOD) of 0.79 (4) mbar and for the 42 mbar case a LOD of 1.68 (7) mbar. The better LOD in the former can be linked to the much longer accumulative acquisition time and larger sample averaging.

Note that the spectra include Raman contributions from nitrogen; these do not originate from within the capillary cell but are generated by laser interaction with atmospheric air outside the cell. Therefore, this signal should be independent

of the pressure conditions within the sample cell, albeit still reflect small changes in the environmental barometric pressure. Indeed, this is the case; normalising the spectra to equal signal acquisition time, the N_2 Q_1-branch peak exhibits the same amplitude (see Figure S11). Thus, this Raman feature can be utilised as an independent reference when determining the SNR and LODs for the gas components inside the capillary.

The spectra shown here were recorded with the *SP500i* spectrometer / *Pixis 400B* detector combination, prior to the implementation of the various fluorescence reduction measures described in this publication. Certainly, all sensitivity and LOD values could be improved upon when incorporating those in full.

It is worth noting that the 5 mbar H_2-example was recorded with a particular scenario in mind. Ultimately, a specific goal at TLK is the measurement of tritiated gas components. For this a purpose-built tritium-compatible capillary Raman system has been set up. To operate such a system without the need to place it within a secondary safety enclosure, the activity inside the capillary system volume should not exceed 10^{10} Bq. For our system that corresponded to ~5 mbar partial pressure for T_2; hence the proof-of-principle test using 5 mbar of H_2 initially. First results of said measurements with tritium have now been successfully completed;[14] the results are broadly in agreement with the detection limits which were deduced from the data in Figure S11.

S2.3 Composition changes during gas circulation and catalytic conversion – a time-lapse movie

We demonstrated that, when using the capillary Raman enhancement setup, the speed, sensitivity and detection limit of acquiring spectra was sufficient to monitor gas mixing processes and catalytic conversion of gas components.

In this work, H_2 and D_2 were injected (gradually) into the capillary system, and Raman spectra were recorded to follow the formation of the isotopologue HD in near real time when the two pure gases were circulated over a platinum-based catalyst.

In Figure 5 of the main manuscript an example of the relative abundance of the three isotopologues during a full sequence of preparing, filling and circulating the aforementioned gas mixtures including catalytic conversion is shown. A detailed description of the numbered sequence described in the figure (phases 1 to 7) is shown here to explicitly describe the gas circulation procedure.

First, the capillary cell and the complete loop were evacuated (phase 2 in the sequence) to remove any gas from a previous measurement (phase 1). During the vacuum pumping all valves were open, to clear the complete system. After about 60 s the vacuum pump was isolated, then waiting for another 60 s to see whether the loop was leaking. Finally, all valves were closed and the procedure to fill the first buffer vessel R1 with deuterium gas commenced.

For the D_2 filling process shown here (phase 3) we did not follow the "calibrated" approach insofar that rather than only filling the reference vessel R1 and then isolating it, the capillary segment up to valves V3 was left connected (*i.e.* valve V4 was left open). Admittedly this procedure generates a "surplus" of D_2 in the system, because cell and tube volumes are added to the reference volume R1. However, this was done to demonstrate that sudden changes in pressure could be recognised in the Raman spectra, when additional gas was admitted into the system via valve V6a. Sudden filling steps are clearly recognisable; at 1000 mbar the process was stopped, closing valves V1a and V4 to now isolate the D_2-filled system.

During the measurement phase 4 (note that only D_2 is present in the capillary, and thus only its Raman feature is observed), the second reference vessel R2 was filled with hydrogen. For this, first the filling pipes and the vessel were evacuated again. Then the vessel was filled with H_2 (valve V2a open), also to a pressure of 1000 mbar; afterwards the filling valve V6b was closed. At the end of phase 4, H_2 was admitted to the capillary cell by opening valve V4. In addition, in preparation for the circulation phase, valves V1a, V1b, V2b and V3c were opened. A drop / increase in the D_2 and H_2 signals were seen when the two gases start to mix, and fill previously evacuated segments of the loop as well.

Then, at the beginning of phase 5, the circulation pump was switched on. This introduced an initial pressure surge in the capillary (P2 indicated a pressure about 20% higher than the initial mixed-filling pressure of about 1000 mbar). This was expected since the capillary with 1 mm inner diameter constitutes a noticeable pump cross section restriction with respect to the tubing of the loop, with 4 mm inner diameter. The circulation was run for about a minute to stabilise.

In the following phase 6, the catalyst vessel was switched into the loop, by quickly opening valves V3a and V3b, and closing V3c. As is evident in the time record, the isotopologue HD started to appear rapidly while D_2 and H_2 diminished as a consequence of the catalytic conversion. The conversion process was complete, *i.e.* the relative abundance of the three isotopologues equilibrates, after about 6.5-7.0 s. Taking into account the total system volume of ~700 cm^3 and the pumping speed of the MB-158E circulation pump of ~365 cm^3/s, nearly full catalytic conversion of the gas mixture was reached after just three circulations of the gas volume through the catalytic converter. Some minor variations in the relative concentration can still be observed, being associated with differential pumping and leakage effects.

Finally, the circulation pump was switched off, and the static mixture was left for further monitoring (phase 7). Note the gradual drop in pressure as the gas equilibrates again through the complete system.

The spectral intensity data shown in Figure 5 of the main manuscript can be converted into partial pressure information. Based on the filling of the H_2 and D_2 reservoirs to 1000 ± 3 mbar, the final overall pressure in the circulating system, parts of which were still evacuated prior to the onset of circulation, was measured to be 838 ± 5 mbar at the end of the catalytic mixing procedure. In the calculations we set the Raman response of each isotopologue as identical (which in reality it is not but at the time of writing absolute response calibration of the *SP500* spectrometer system had not yet been completed). We derived a detection limit (SNR = 3) for the hydrogen isotopologues of 2.3 ± 0.4 mbar – averaged over

a series of three repeat measurements – for an acquisition time of just 2×0.5 s. Therefore, relative isotopologue changes of ~1 mbar/s could be traced. This can be viewed as confirmation that, in principle, the approach could be suitable for rapid process control.

In order to visualise the evolution of the full set of spectral features in the gas mixing / conversion process, rather than only to plot the changes in Q_1-branch amplitudes (as displayed in Figure 5 in the main text), all spectra have been collated into a real-time time-sequence "video". Into this sequence appropriate procedural sketches are introduced, which provide conceptual guidance of how the mixing and catalytic conversion processes have been implemented.

Note that in order to keep the movie to a reasonable length, out of the complete run of just over 15 minutes various segments have been removed during which no pressure and / or signal changes were expected or observed.

References

1. K. Izutsu, Y. Hiyama, C. Yomota and T. Kawanishi; "Near-infrared analysis of hydrogen-bonding in glass- and rubber-state amorphous saccharide solids", *Pharm. Sci. Tech*. 2009, **10**, 524-529.
2. J. Etchepare, M. Merian and L. Smetankme; "Vibrational normal modes of $Si0_2$: I. α and β quartz", *J. Chem. Phys*. 1974, **65**, 1873-1876.
3. N. Tomozeiu; "Silicon Oxide (SiO_x, 0<x<2): a Challenging Material for Optoelectronics", in "*Optoelectronics - Materials and Techniques*", P. Predeep (ed), InTech Europe, Rijeka, Croatia, 2011, ISBN 978-953-307-276-0.
4. J. Sils, S. Hausfeld, W. Clauß, U. Pahl, R. Lindner and M. Reichling; "Impurities in synthetic fluorite for deep ultraviolet optical applications", *J. Appl. Phys*. 2009, **106**, 063109.
5. J.C. Mullen, M.P. Buric and S.D. Woodruff; "Azimuthal polarization for Raman enhancement in capillary waveguides", *Opt. Eng*, 2013, **52**, 117103.
6. M. Schlösser, B. Bornschein, S. Fischer, T.M. James, F. Kassel, S. Rupp, M. Sturm and H.H. Telle, "Raman spectroscopy at Tritium Laboratory Karlsruhe", *Fusion Sci. Technol*., 2015, **67**, in press.
7. S.A. Danichkin, A.A. Eliseev, T.N. Popova, O.V. Ravodina and V.V. Stenina; "Raman scattering parameters for gas molecules (survey)", *J. Appl. Spectrosc*, 1981, **35**, 1057-1066
8. C.M. Penny and M. Lapp; "Raman scattering cross sections for water vapour", *J. Am. Soc. Am*. 1976, **66**, 422-425.
9. Kaye & Laby Online; "Tables of Physical and Chemical Constants: 3.1.4 Composition of the Earth's Atmosphere", v2.0 / 16 Oct 2012, www.kayelaby.npl.co.uk [last accessed on 30 June 2014].
10. (a) J.M. Eiler; "Clumped-isotope geochemistry – The study of naturally-occurring, multiply-substituted isotopologues", *Earth Planet. Sci. Lett*. 2007, **262**, 309-327.
    (b) J.S. Coursey, D.J. Schwab, J.J. Tsai and R.A. Dragoset; "Atomic weights and isotopic composition with relative atomic masses", NIST Physical Measurement Labora-tory, Gaithersburg, MD 20899-8400, USA, **2013**. http://www.nist.gov/pml/data/comp.cfm Date created: 23 August 2009; last updated: 15 May 2013.
11. T.M. James, M. Schlösser, R.J. Lewis, S. Fischer, B. Bornschein and H.H. Telle; "Automated quantitative spectroscopic analysis combining background subtraction, cosmic ray removal, and peak fitting", *Appl. Spectrosc*. 2013, **67**, 949-959.
12. M. Schlösser, S. Rupp, H. Seitz, S. Fischer, B. Bornschein, T.M. James and H.H. Telle; "Accurate calibration of the laser Raman system for the Karlsruhe Tritium Neutrino Experiment", *J. Mol. Struct*. 2013, **1044**, 61-66.
13. T. Padfield; "Fundamental microclimate concepts", in '*Conservation Physics - an online textbook*', http://www.conservationphysics.org/intro/fundamentals.php . [last accessed on 05 July 2014]
14. S. Rupp, T.M. James, H.H. Telle, M. Schlösser and B. Bornschein; "Enhanced sensitivity of Raman spectroscopy for tritium gas analysis using a metal-lined hollow glass fiber", *Fusion Sci. Technol*., 2015, **67**, in press.